Weierstraß-Institut
für Angewandte Analysis und Stochastik

im Forschungsverbund Berlin e.V.

Preprint ISSN 0946 – 8633

Simulation of Phase-Controlled Mode-Beating Lasers

Hans-Jürgen Wünsche[1,3] , Mindaugas Radziunas[2] , Stefan Bauer[3] ,

Olaf Brox[3] , Bernd Sartorius[3]

submitted: 24 Jan 2003

[1] Humboldt-Universität zu Berlin
Institut für Physik
Invalidenstr. 110
D – 10115 Berlin
Germany
E-Mail: wuensche@physik.hu-berlin.de

[2] Weierstraß-Institut
für Angewandte Analysis und Stochastik
Mohrenstrasse 39
D – 10117 Berlin
Germany
E-Mail: radziuna@wias-berlin.de

[3] Fraunhofer-Institut für Nachrichtentechnik
Heinrich-Hertz-Institut
Einsteinufer 37
D – 10587 Berlin
Germany
E-Mail: bauer@hhi.de, brox@hhi.de, sartorius@hhi.de

No. 809
Berlin 2003

2000 *Mathematics Subject Classification.* 78A60,78-05,35-04.

Key words and phrases. semiconductor laser, distributed feedback, modelling, self-pulsations, high speed, all optical signal processing, 3R-regeneration .

Edited by
Weierstraß-Institut für Angewandte Analysis und Stochastik (WIAS)
Mohrenstraße 39
D — 10117 Berlin
Germany

Fax: + 49 30 2044975
E-Mail: preprint@wias-berlin.de
World Wide Web: http://www.wias-berlin.de/

Abstract

Self-pulsations in Phase Controlled Mode Beating lasers (PhaseCOMB) are very attractive for all-optical clock recovery at ultra-high bit rates. In this paper we apply the comprehensive simulation tool LDSL that has been developed by us for studying the self-pulsation features of PhaseCOMB lasers considering the effects of spontaneous emission noise, longitudinal spatial hole burning, and gain dispersion. In particular the importance of mode control for adjusting the PhaseCOMB operating conditions is pointed out. The simulation results are confirmed by measurements on fabricated devices.

1 Introduction

The dramatic growth of internet traffic pushes the interest in high speed all-optical signal processing. One key function is 3R-regeneration (**r**eamplification, **r**etiming, **r**eshaping) [1]. Realizations of this function up to 80 GHz using self-pulsating lasers for clock extraction have been reported (e.g., [2]). To achieve such very high frequencies, which considerably exceed the relaxation oscillation frequency, a new operation principle has to be used.

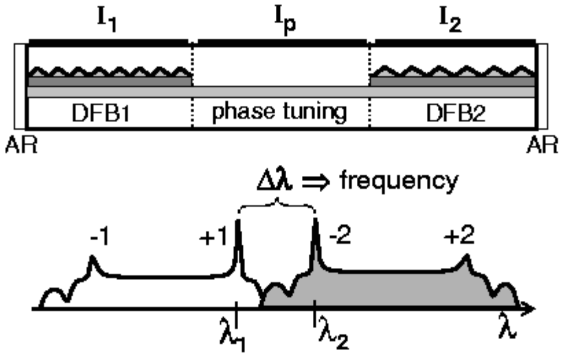

Figure 1: *Sketch of a PhaseCOMB laser and of its operation principle.*

The exploited self-pulsations by Phase Controlled Mode Beating (PhaseCOMB) are based on three-section lasers comprising two DFB sections, detuned by about the stop band width, and an integrated phase tuning section. The two adjacent inner DFB modes are selected for lasing via the phase tuning section (Fig. 1). Beating of the two coupled modes leads to the wanted self-pulsation with a frequency determined by the spectral separation of the lasing modes. This basic operation principle of the PhaseCOMB has been confirmed already in [3] by numerical simulation in comparison with first fabricated devices.

The present paper reports on modelling calculations having accompanied the further development of these devices. A central question of this work is the proper selection of the two beating modes. In this context, we focus our presentation on the role of effects which were not considered in [3]. These effects are spontaneous emission noise, longitudinal spatial hole burning (LSHB), and gain dispersion.

The paper is organized as follows. In the next section we briefly review the model equations for multisection DFB PhaseCOMB laser with incorporation of the new effects. The specific influences of noise and LSHB are evaluated in Sections 3 and 4, respectively. Comparison with measurements is given in Section 5 for a selected device. Section 6 investigates how to improve the mode control by utilizing the gain dispersion. The paper ends with a conclusion.

2 Traveling wave model

Our previous analysis of PhaseCOMB lasers [3] is based on the traveling wave model of Ref. [4]. For the present investigation, our software tool LDSL (**L**ongitudinal **D**ynamics in **S**emiconductor **L**asers) is extended to incorporate additionally spontaneous emission noise, nonlinear gain saturation, gain dispersion, and longitudinal spatial hole burning (LSHB). In the following, we describe briefly, how these effects are contained in the equations underlying the present version of LDSL.

The optical field $E(z,t) = (E^+(z,t), E^-(z,t))$ is represented by the slowly varying amplitudes of the optical fields traveling forward (+) and backward (-) along the longitudinal axis of the device ($z \in [0, L]$). They are governed by the well-known traveling wave equations (TWE)

$$-i\frac{n_g}{c}\partial_t E^{\pm} \;=\; \Big(\pm i\partial_z - \beta\Big)E^{\pm} - \kappa E^{\mp} + F^{\pm}_{\mathrm{sp}}, \qquad (1)$$

with the boundary conditions $E^+(0,t) = E^-(L,t) = 0$ at the anti-reflection (AR) coated facets. By proper normalization, $|E(z,t)|^2 = |E^+|^2 + |E^-|^2$ is a local photon density (local power at z divided by the global constant $\hbar\omega_0 v_g A_{\mathrm{AZ}}$). $n_g = c/v_g$ and β describe the group velocity and the linear propagation properties of the fundamental transverse mode of the internal waveguide at a central wavelength λ_0, respectively. The counterpropagating waves are mutually coupled with strength κ. The quantities $F^{\pm}_{\mathrm{sp}}$ represent the spontaneous emission contributions to be described in Section 3.

The parameter models for the active and passive sections are different. In the passive middle section, κ and $F^{\pm}_{\mathrm{sp}}$ disappear and the propagation parameter is a constant that we express by the round trip phase shift φ over the sectional length L_p and an optical loss coefficient α as

$$\beta = -\frac{\varphi}{2L_p} - i\frac{\alpha}{2} \qquad \text{(passive section).} \qquad (2)$$

In the active DFB sections, the model for the propagation parameter is

$$\beta = \delta - i\frac{\alpha}{2} + (i + \alpha_H)\frac{g}{2} + i\mathcal{D} \qquad \text{(active sections).} \qquad (3)$$

The constant $\delta = -\Delta \cdot 2\pi n_g/\lambda_0^2$ is determined by the static wavelength detuning Δ of the stop band center from the central wavelength λ_0. α_H is the linewidth enhancement factor. The contribution $\mathcal{D}$ incorporates dispersion effects to be specified in section 6. The spectral gain maximum is assumed to depend on carrier density n and photon density $|E|^2$ according to

$$g(n, \varepsilon|E|^2) = \frac{g'(n - n_{tr})}{1 + \varepsilon|E|^2} \tag{4}$$

with the gain slope g'. A linear relation between g and n is sufficient, because we consider bulk active zones and n covers only a limited range in a PhaseCOMB laser. Taking into account a nonlinear saturation coefficient ε is also new compared to [3, 4], however, it is only of marginal influence and we shall not discuss it furthermore.

The evolution of the carrier densities in active sections is described by the rate equation

$$\partial_t n = \mathcal{I} - R(n) - \frac{c}{n_g}\, \Re e[E^*(g + 2\mathcal{D})E]. \tag{5}$$

$R(n) = An + Bn^2 + Cn^3$ is the usual polynomial recombination law. In contrast to our former model [4, 3], the stimulated recombination (last term) is not averaged over one section. Hence, we allow now for densities varying also with z (spatial hole burning). In this context, the injection rate $\mathcal{I}$ becomes inhomogeneous, too, as will be specified in section 4.

The calculations to be presented base on the parameter values collected in Table 1, deviations will be noted. It is the parameter set of Ref. [3] supplemented by additional parameters needed in the extended model. Note that g', ε, and $\bar{g}$ already incorporate the transverse confinement factor Γ.

3 Spontaneous Emission Noise and Jitter

Spontaneous emission is described by the Langevin forces $F_{\mathrm{sp}}^{\pm}$ in the TWE (1) with the correlation functions

$$\langle F_{\mathrm{sp}}^{+*}(z,t) F_{\mathrm{sp}}^{+}(z',t')\rangle = \langle F_{\mathrm{sp}}^{-*}(z,t) F_{\mathrm{sp}}^{-}(z',t')\rangle = \delta(z-z')\,\delta(t-t')\,\frac{n_g}{c}\beta_{\mathrm{sp}} R. \tag{6}$$

All other correlation functions as well as the expectation values of $F_{\mathrm{sp}}^{\pm}$ vanish. β_{sp} is the relative portion of spontaneous recombination emitted into the guided wave. The recombination rate R is taken here at the transparency concentration, for simplicity. The stochastics of these quantities is realized in the numerics by appropriately using the random number generator. A typical example for a calculated SP is given in Fig. 2a. The pulse shape is nearly sinusoidal, only weakly perturbed by noise and exhibits a good extinction. The pulses emitted from the two facets differ slightly and are shifted relative to each other by nearly half a period.

Table 1: Parameter values

	explanation	values	unit
	length of DFB sections	250	μm
L_P	length of phase section	400	μm
n_g	group velocity index	3.4	
κ	DFB coupling coefficients	130	cm^{-1}
Δ_1	grating detuning DFB1	$+1.0$	nm
Δ_2	grating detuning DFB2	-3.4	nm
α	DFB internal absorption	25	cm^{-1}
α_P	phase section absorption	20	cm^{-1}
α_H	Henry factor	-4	
g'	differential gain	7	10^{-17} cm^2
n_{tr}	transparency carrier density	1	10^{18} cm^{-3}
ε	gain compression factor	3	10^{-18} cm^3
A	recombination coefficient	3	10^8 s^{-1}
B	recombination coefficient	1	10^{-10} cm^3/s
C	recombination coefficient	1	10^{-28} cm^6/s
β_{sp}	spontaneous emission factor	10^{-4}	
A_{AZ}	cross section of active zones	4.5	10^{-9}cm^2
I	current injection, DFB section	90	mA
U'_F	differential Fermi voltage	5	$10^{-20}\text{V}/\text{cm}^3$
R_s	series resistivity	10	Ω
λ_0	central wavelength	1570	nm
$\bar{g}$	Lorentzian gain amplitude	10	cm^{-1}
λ_G	gain peak detuning	0	nm
$2\Delta_G$	FWHM of gain curve	90	nm

Although the spontaneous emission is only a small perturbation it has remarkable qualitative consequences. Without spontaneous emission, self-pulsations are periodic oscillations of the output intensity. Taking the randomness of the spontaneous emission into account, any periodicity in the strong sense is lost. Short term intensity fluctuations appear as well as a long term random drift of the pulse positions relative to the 'average period' causing e.g. unwanted jitter within the sequence of pulses.

For the application as optical clock, all noise phenomena should be kept small. In order to compare different designs and points of operation, we evaluate the according quality of calculated self-pulsations by the mean frequency f and a rms-jitter parameter J, determined in the following way.

First, we look for the mean period T of the self-pulsations. To estimate T, we locate the times t^i_{up} when the increasing i-th pulse slope crosses the mean output power value. A straight line through these points (least square fit) gives a best estimate of the mean period T and of the mean frequency $f = 1/T$.

By sampling the pulses with period T, the eye and pulse drift diagrams shown in

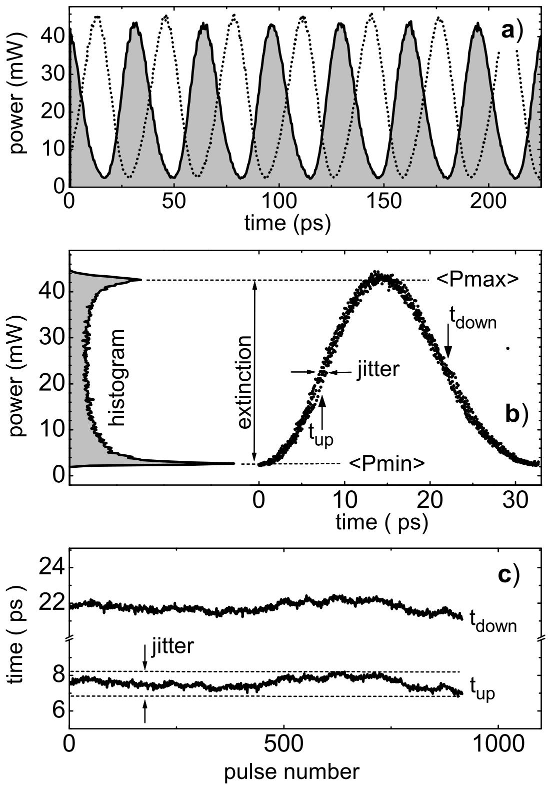

Figure 2: *Characterisation of a typical calculated self-pulsation (phase shift $\varphi = 0.6$).*
a) Part of the pulse train. Full: front facet (DFB1). Dotted: back facet (DFB2).
b) Eye diagram and power distribution histogram.
c) Temporal positions of the up and down half-heights along a 30 ns pulse train, exhibiting a maximum jitter of about 1.5 ps.

Figs. 2b and 2c are obtained. The variance σ of the distribution of half height points is used to determine the rms-jitter parameter according to

$$J = -10\lg(2\sqrt{2\ln 2}\,\sigma/T). \tag{7}$$

It is about 20 dB in the present example, corresponding to a half width of the t_{up} distribution of about 1% of the pulsation period, i.e., $\approx$300 fs. Note that the full variation of t_{up}(horizontal lines in Fig. 2c) is much bigger, about 1.4 ps in our case. These values are acceptable for the application of the device as an optical clock. The dependence of J on different regimes of operations is given by the thin solid lines in Fig. 6. For the 40 GHz and 80 GHz bands, we find always $J \approx 20$ dB. We conclude that the jitter of SPs with frequencies in this range is reasonably low in our devices and nearly independent of the point of operation.

Another consequence of noise is to drive weakly damped side modes as well as to stimulate parasitic oscillations of the nonlinear system, e.g., relaxation oscillations. Such effects in turn can degrade the jitter and extinction of the SP. To analyze them, we calculate optical and RF spectra. Fig. 3 gives examples for the point of operation of Fig. 2.

The optical spectrum in Fig. 3a is obtained from the Fast Fourier Transform of $E^+(L,t)$ with 2^{15} sampling points and averaged with a resolution of about 0.04 nm. It shows the two lasing modes labeled +1 and -2, their four wave mixing products (labeled 4wm), side modes labeled by -1, -2b, +2, and smaller resonances. Here and in the following, the labels attribute peaks to DFB modes as already sketched in Fig. 1. The peak -2b corresponds to a hole-burning induced side mode to be discussed in the next section. When switching off spontaneous emission, the noise floor and the side modes disappear from the spectrum.

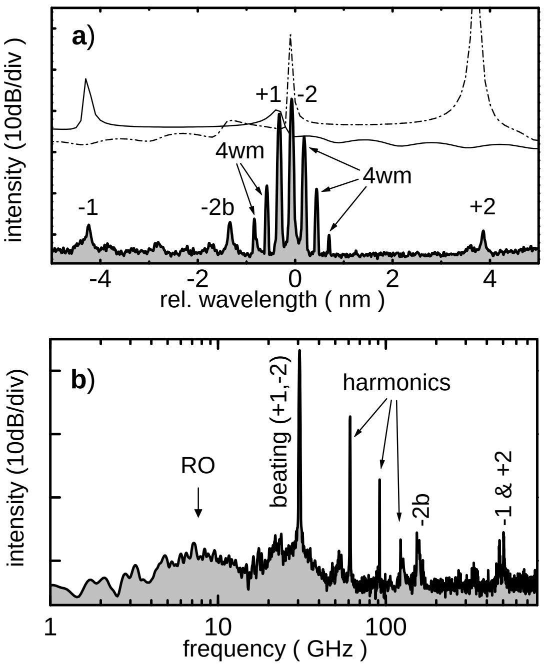

Figure 3: *Spectra of the operation point of Fig. 2.*
a) Optical spectrum. The main DFB modes are labeled according to Fig. 1. Label -2b indicates a LSHB enhanced side mode according to Section 4, Fig. 5b. By 4wm the four-wave mixing products of the two beating modes +1 and -2 are labeled.
b) RF spectrum. RO: damped relaxation oscillation, beating (+1,-2): main self-pulsation, -2b: beating of the corresponding side mode in the optical spectrum with the lasing modes, -1 & +2: beating of opposite DFB modes with lasing modes. The harmonics belong to the main self-pulsation.

The presence of noise driven side modes can also be detected in the RF spectrum, Fig. 3b. It has been calculated by fast Fourier transforming $|E^+(L,t)|^2$ using 2^{15} sampling points within 22 ns. The result is averaged with a resolution of about 400 MHz and 800 spectra have been averaged for smoothing. Most prominent lines are the beating self-pulsation and its harmonics. Without noise, only these lines are present. Noise introduces a back ground between the lines with additional side peaks on top. At low frequencies, the peak labeled RO is caused by noise induced relaxation oscillations. They also cause lower-frequency satellites of the most intense beating lines. The line pairs above 100 GHz correspond to the beating of the two lasing modes with the side modes indicated by the labels. Due to the limited range of detectable frequencies, they are not observable in experimental RF spectra. However, they can act as perturbations in a communication system.

Summarizing this section, spontaneous emission noise is included into the modelling and tools are developed for analyzing the impact on the jitter of self-pulsations. For the present device a rms timing jitter of about 300 fs within a time interval of 30 ns is calculated, only weakly depending on the point of operation. The effect of noise on optical spectra and power rf spectra is investigated too. The noise enhances unwanted DFB modes resulting in reduced side mode suppression in optical spectra and it feeds relaxation oscillations in the laser leading to an increasing noise floor in the corresponding frequency range of the rf spectrum. Via both effects the timing stability of the self-pulsation is degraded. Our modelling tool will be very helpful in optimising the devices for low jitter.

4 Spatial Hole Burning and Mode Control

Along a DFB laser, the photon density is not uniform but has a distinct maximum in the interior of the device. The corresponding local peak of the stimulated recombination causes a local decrease of the carrier density. This effect is usually called longitudinal spatial hole burning (LSHB). An example of the LSHB in a PhaseCOMB laser is given in Fig. 4.

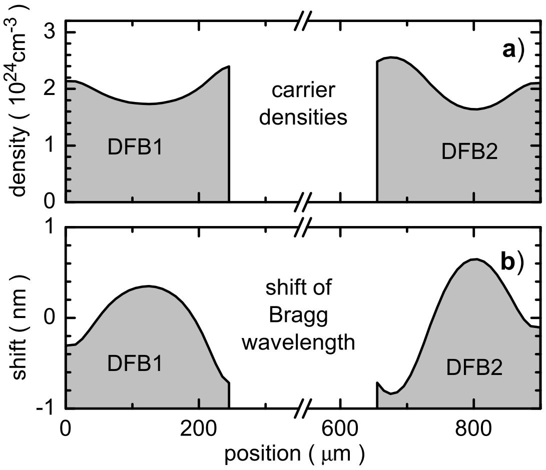

Figure 4: *Axial distributions in a PhaseCOMB laser with phase shift* $\varphi/2\pi = 0.6$.
a) carrier densities.
b) wavelength shift of the Bragg resonance.

A quantitative description of LSHB requires to take into account the current self-distribution (CSD): the injection current density becomes also inhomogeneous in order to ensure a constant voltage along the electrical contact [5, 6, 7, 8]. To this purpose, we use the model

$$\mathcal{I}(z,t) = \frac{I}{eV} - \frac{U_F'}{eVR_s}(n(z,t) - \bar{n}(t)) \tag{8}$$

for the injection rate of Equ. (5). The first term determines the average injection rate by the constant injection current I and the active volume V of the section. The second term is the CSD contribution linearized with respect to the deviation of the density from its spatial mean value $\bar{n}(t)$ beneath a given electrical contact. The derivative of the Fermi level separation U_F' and the series resistivity R_s are treated as constant parameters.

4.1 Single section DFB laser

Let us first briefly consider the simple case of a solitary DFB laser (with parameters of the section DFB2). Of course, the impact of LSHB depends on the injection level. The results of calculations drawn in Fig. 5 exhibit multiple qualitative changes (bifurcations). Bifurcation A at 32 mA is the laser threshold. Below it, the carrier density remains homogeneous. At threshold, the density dip in the device center begins to appear. With raising injection, this dip deepens. This is accompanied by an increase of the densities at the facets, but the mean density (not plotted) remains nearly constant. At the next bifurcation B at 75 mA, the symmetric solution looses stability and two new solutions with asymmetric density profiles (each one the mirror of the other) become stable. This symmetry-asymmetry pitchfork bifurcation has first been predicted by Schatz [9]. At the same time, the mean density of now asymmetric distribution of carriers starts to grow much faster, what can be also recognized from the growth of the density value in the center of section (see Fig. 5a). At about 99 mA, the stationary laser state looses stability in the bifurcation C. Beyond it, self-pulsations of about 1 GHz repetition rate appear. These LSHB self-pulsations have been discovered by Lowery [10]. The currents for the bifurcations B and C decrease with increasing Henry factor α_H. Fig. 5 was calculated with $\alpha_H = -6$. To avoid the unwanted effects above bifurcation B, the driving currents should be limited to values below 100 mA.

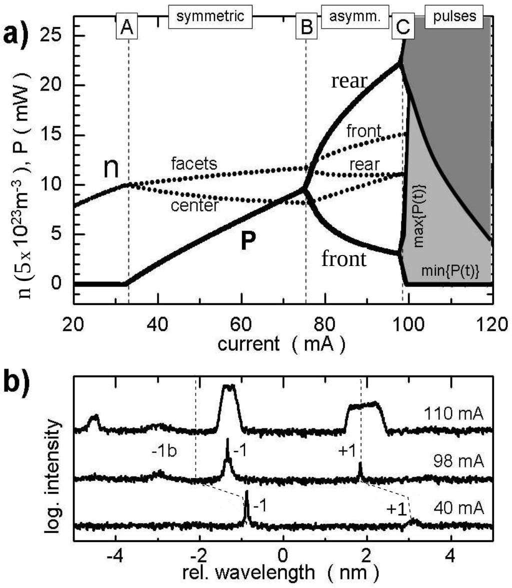

Figure 5: *Dependence of effects of LSHB in a single-section DFB laser on injection current. Parameter as DFB2 in Table 1 except $\alpha_H = -6$.*
a) Full: maximum and minimum output power within a simulation interval of 20 ns at front and rear facets. Dashed: carrier density at the facets and in the center of the device.
b) Examples for the optical spectra in the different current ranges. Dashed lines show approximate location and changes of the stop band.

However, even at small currents, LSHB has a considerable impact on optical spectra as illustrated in Fig. 5b. First, due to significant growth of the mean carrier density after crossing bifurcation point B, the blue shift of the stopband can be observed (see thin dashed lines in Fig. 5b). Next, the inhomogeneous carrier density causes a corresponding longitudinal variation of the index of refraction. The Bragg resonance of the grating thus has not the identical spectral position along the section (Fig. 4). In our examples, it varies over nearly 2 nm, a considerable portion of the stop band. The symmetry of the stop bands is therefore lost and the laser preferably operates on the mode -1 on the short wavelength side of its stop band as it is shown in Fig. 5b. For the type of operation sketched in Fig. 1, this effect of LSHB may perturb, because we need one laser to operate on the long wavelength mode. With increasing injection, mode -1 shifts into the stop band because it is located in the center of the device where the Bragg resonance shows a redshift. At the same time, a short wavelength side mode -1b grows up that profits more from the facet regions. Under some conditions, even both these modes can participate in the lasing. In the pulsation regime above bifurcation C, the spectra become broadened and clear indication is given for the multimode nature of this pulsation, in concordance with Ref. [10].

4.2 PhaseCOMB laser

Control of the two beating modes by the phase shift φ of the middle section is essential for the proper operation of a PhaseCOMB laser. To study the impact of LSHB on this effect, we compare in Fig. 6 the dependence of beating frequencies on φ calculated without and with LSHB.

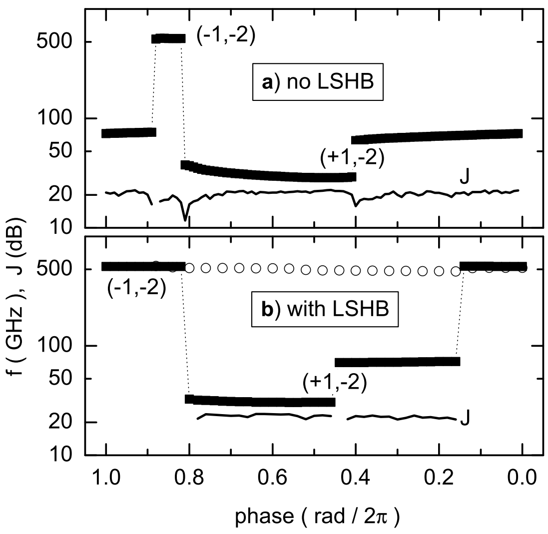

Figure 6: *Calculated beating frequencies (thick) and jitter (thin solid line) versus phase parameter φ.*
a) Without LSHB as in Ref. [3].
b) With LSHB. Black: parameter of Table 1. Open circles: frequencies calculated with changed parameters $\alpha_H = -6, \alpha = 40\ cm^{-1}, L_1 = L_2 = 270\,\mu m$.

Without LSHB, the wanted DFB modes +1 and -2 are beating over nearly 90% of a phase period. This range is splitted into two frequency plateaus, one with frequencies between 30 GHz and 40 GHz, the other one at about 80 GHz. This splitting is due to the superimposed FP-type mode comb of the internal resonator formed by the phase section [3]. The third plateau in the phase range between 0.8 and 0.9 is connected with a wrong mode selection. In this small interval, both short wavelength DFB modes are lasing. The according beating frequency of about 540 GHz corresponds to the assumed 4.4 nm grating detuning.

Now we turn to the cases with LSHB. We know from the single section laser that LSHB prefers the short wavelength DFB mode. Thus, we can expect that the phase range with the wrong mode selection will increase. Fig. 6b confirms this speculation. Nevertheless, for a laser with parameters of Table 1 there is still a comfortable interval with the wanted mode selection. However, the extension of this interval depends sensitively on the length of the sections, on α_H and on the internal optical losses α. To estimate possible consequences, we have repeated the calculations for a slightly worse configuration. In this case (open circles), the device operates in the wrong mode constellation for all phase shifts and could not be used for applications at e.g. 40 GHz. We draw the conclusion that these parameters should be carefully controled to ensure a proper operation of PhaseCOMB devices.

5 Comparison to Experiment

To verify the results obtained from modelling we fabricated devices with $\kappa = 130$ cm^{-1} comparable to simulation. The phase section length is fixed to 300 μm whereas the length for each DFB section can be defined individually by cleaving them in the desired geometry. The gratings of the investigated lasers were detuned by 4.8 nm. Each laser is AR coated on both facet with a residual power reflectivity of 10^{-4}. As the control parameters - i.e. the currents - of a realized device require a large number of measurements, we have automatized this work.

The measurement setup looks as follows. The light emitted from the device is coupled into a tapered fiber and an isolator is used to suppress back-reflections from other optical devices. All three driving currents are computer controlled and at each measurement point a full optical spectrum is recorded. To reduce the amount of data we first focus on symmetrical pumping of the DFB currents in a range from 20 to 100 mA in steps of 5 mA. For each DFB current we vary the phase current between 0 and 20 mA to see the influence of the phase on the coupling of both DFBs. For a quick overview a grey scale intensity plot for a DFB current pair is used (cf. Figs. 7b and 8b). A horizontal cut at a distinct phase current corresponds to the respective optical spectrum. As the driving currents do not only influence the optical intensity but also the emission wavelength due to thermal effects, we assess its influence by repeating the described measurement for different current weighting.

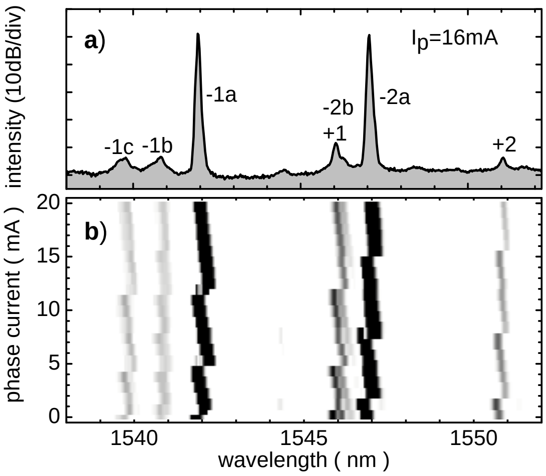

Figure 7: *Mode characteristics of device 1 measured at $I_1 = 85$ mA and $I_2 = 90$ mA.*
a) Optical spectrum at 16 mA phase current.
b) Top view on the evolution of optical spectra with phase current from 0 to 20 mA. Black: the two lasing modes. Gray scaled: less intense side modes.

To show the impact of high κL values we cleaved devices with a geometry of 270 μm, 300 μm and 270 μm for DFB1, phase and DFB2 section respectively. The overview in Fig. 7 with pumping currents of 85 and 90 mA for DFB1 and DFB2 sections respectively, illustrates the behavior already known from modelling. For the whole range of feedback phases we do not obtain the desired mode beating. Reason is the stable emission of each individual section on its short wavelength mode due to the excessive longitudinal spatial hole burning. This situation remains dominant for all current combinations in the DFB sections.

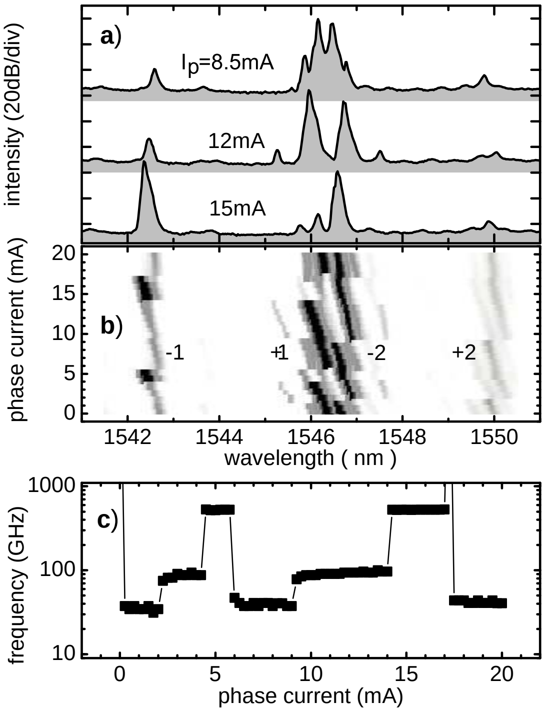

Figure 8: *Mode characteristics of device 2.*
a) and b) as in Fig. 7.
c) Beating frequencies versus phase current as determined from the measured optical spectra.

Nevertheless, one can obtain good mode beating self-pulsations by two coupled DFBs. The strategy has to be a reduction of the spatial hole burning, which implies a κL as small as allowed by the other laser parameters. Fig. 8b shows the measurements for a device with the same parameters as described above, the only difference is a reduced DFB section length of 225 μm each. For the larger part of a phase period we now find the desired emission of the adjacent modes of the DFBs. Concentrating on one phase period arbitrarily picked from 6 to 17 mA three main scenarios are found. Depending on the phase we can switch between 40 GHz and 80 GHz, and only for a small fraction of the phase period the hole burning mode of the short wavelength DFB prevents pulsations. Fig. 8a shows an example for each case. The lower diagram indicates the corresponding beating frequencies versus the phase current. They compare fairly well with the calculated dependencies of Fig. 6.

6 Utilizing the Gain Dispersion

Let us discuss now a possible impact of gain dispersion on the mode selection in a PhaseCOMB laser.

The gain dispersion contribution $\mathcal{D}$ to the propagation constant β in Equ. (3) is a linear operator determined by

$$\begin{aligned} \mathcal{D}E^{\pm} &\stackrel{def}{=} \frac{\bar{g}}{2}(E^{\pm} - p^{\pm}) \\ -i\partial_t p^{\pm} &= -i\bar{\gamma}(E^{\pm} - p^{\pm}) + \bar{\omega}p^{\pm} \end{aligned} \tag{9}$$

This oscillator model for the polarization corresponds to the Lorentzian-shape gain dispersion [11]

$$G(\lambda) \stackrel{def}{=} g - \bar{g}\frac{(\lambda_0 + \lambda_G - \lambda)^2}{(\lambda_0 + \lambda_G - \lambda)^2 + \Delta_G^2}, \tag{10}$$

where g is the maximum gain of Equ. (4), and

$$\lambda_G = -\bar{\omega}\frac{\lambda_0^2}{2\pi c} \quad \text{and} \quad \Delta_G = \bar{\gamma}\frac{\lambda_0^2}{2\pi c},$$

denote the detuning between gain maximum and central wavelength λ_0 and the half width at half maximum of the gain curve, respectively.

Up to here and in our previous simulations in [3], we were neglecting the effects of gain dispersion at all, centering gain curve close to the modes +1 and -2 and assuming very small gain curvature (thin flat curve in Fig. 9a) just to guarantee better convergence of our numerical scheme. We argued this approach by the largeness of the gain region, which usually is quite big (~50-100 nm), and the most important resonance modes ± 1 and ± 2 are located only within small ~5-10 nm interval, where the gain level for all these modes can be approximately the same.

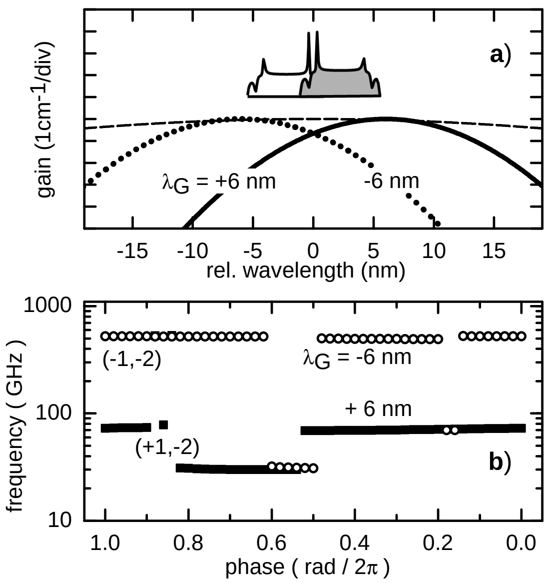

Figure 9: *Impact of gain dispersion to the type of self-pulsations.*
a): different used gain curves and corresponding reflectivity spectra of DFB sections.
b): frequencies of SP in Phase-COMB laser at different phases φ when gain peak is centered at $+6$ (black) and -6 nm (open circles).

Now we remember the message of paper [11]. There it has been demonstrated, that small ~1-3 cm^{-1} differences of gain level can cause the selection of another DFB resonance mode. In order to check these suppositions for PhaseCOMB lasers, now we consider a more realistic stronger gain dispersion by setting $\bar{g} = 150$ cm^{-1}. The resulting changes are small as long as the stop bands are kept on top of the gain curve. But even comparatively small gain detunings show a noticeable effect. To be concrete, we compare the cases $\lambda_G = -6$ nm and $\lambda_G = 6$ nm, respectively (see thick dashed and solid curves in Fig. 9a). These gain curves imply a $\sim$1-2 cm^{-1} gain suppression of longer (shorter) DFB resonance modes with respect to corresponding shorter (longer) DFB resonances, respectively.

This effect can be used to further counteract the LSHB-support of mode -1 by using a gain peak on the longer wavelength side of the stop bands. To this purposes, we apply the $+6$ nm shifted gain dispersion represented by thick solid line in Fig. 9a. In this case, also mode $+2$ is additionally supported, but it is not a problem as long as this mode keeps suppressed by LSHB. The results plotted in Fig. 9b as a thick solid line show indeed the wanted mode selection for nearly all possible phase shifts.

On contrary, an opposite gain detuning (dotted dispersion curve in Fig. 9a) gives a situation, where the mode -1 is supported by both LSHB and gain dispersion, preventing the operation at the required modes (see Fig 9b). Nevertheless, even in this case SP at ~ 30 or ~ 80 GHz frequencies still can be seen at properly selected phase conditions.

As the consequence of the discussion above, we conclude, that operating the laser on the short wavelength side of the gain maximum can counteract the LSHB induced oscillation of the shortest wavelength mode -1.

7 Conclusion

In this paper the numerical simulation tool LDSL is extended and applied for studying the quality of self-pulsations in PhaseCOMB lasers. In particular the impact of two main perturbations in realistic devices is investigated: spontaneous emission noise and longitudinal spatial hole burning. As expected, noise leads to jitter of the self-pulsation. The calculated jitter is typically only a few percent of the pulse period (some hundred fs), nearly independent of the point of operation. Spatial hole burning turns out to be the more critical effect. It supports lasing on the short wavelength stop band mode which can lead to loss of the operating conditions needed for phase controlled mode beating pulsations. Short DFB lengths, low optical losses, a low linewidth enhancement factor, and setting the DFB grating on the short wavelength side of the gain maximum are measures to avoid this negative effect. Simulation results are compared with and confirmed by measurements on fabricated devices.

Acknowledgments

This work has been supported by Deutsche Forschungsgemeinschaft (DFG). It was also supported by Bundesministerium für Bildung und Forschung (BMBF) project No. 13N79789. Experiments have been performed in the framework of the Research Partner Program of Alcatel.

References

[1] P. Brindel, B. Dany, D. Rouvillain, B. Lavigne, P. Guerber, E. Balmefrezol, O. Leclerc "All-Optical Signal Regenerators for Ultra-High Bit-Rate Transmission Systems", IEICE Transactions on Electronics, vol. E85-C, no. 1, pp. 126-134, Jan. 2002.

[2] C. Bornholdt, S. Bauer, M. Möhrle, H.-P. Nolting, B. Sartorius, "All-optical clock recovery at 80 GHz and beyond," *Proc. ECOC* 2001, Amsterdam (NL), p. 502.

[3] M. Möhrle, B. Sartorius, C. Bornholdt, S. Bauer, O. Brox, A. Sigmund, R. Steingrüber, M. Radziunas, H.-J. Wünsche, "Detuned Grating Multisection-RW-DFB Lasers for High Speed Optical Signal Processing", *IEEE J. Sel. Top. Quantum Electron.*, vol. **7**, pp. 217-223, 2001.

[4] M. Radziunas, H.-J. Wünsche, B. Sartorius, O. Brox, D. Hoffmann, K. Schneider, and D. Marcenac, "Modeling Self-Pulsating DFB Lasers with an Integrated Phase Tuning Section", *IEEE J. Quantum Electron.*, vol. **36**, pp. 1026-35, 2000.

[5] U. Bandelow, H. Wenzel and H.-J. Wünsche, "Influence of inhomogeneous injection on sidemode suppression in strongly coupled DFB semiconductor lasers", *Electronics Letters*, vol. 28, pp. 1324-25, 1992.

[6] Yves Champagne and Nathalie McCarthy, "Influence of the axially varying quasi-Fermi-level separation of the active region on spatial hole burning in distributed-feedback semiconductor lasers", *Journal of Applied Physics* vol. 72, pp. 2110-2118, 1992.

[7] P. G. Eliseev and A. E. Drakin, "Self-distribution of the current in laser diodes and its possible use for reducing the optical nonlinearity of the active medium", *Quantum Electronics* **26**, pp. 299-302, 1996.

[8] P. G. Eliseev, A. G. Glebov, and M. Osinski, "Current self-distribution effect in diode lasers: analytic criterion and numerical study", *IEEE Journ. Select. Topics Quant. Electron.* vol. 3, pp. 499-506, 1997.

[9] R. Schatz, "Longitudinal spatial instability in symmetric semiconductor lasers due to spatial hole burning", *IEEE Journ. Quant. Electron.* vol. 28, pp. 1443-49, 1992.

[10] A. J. Lowery, "Dynamics of SHB-induced mode-instabilities in uniform DFB semiconductor lasers", *Electron. Lett.* vol. 29, pp. 1852-53, 1993.

[11] U. Bandelow, M. Radziunas, J. Sieber, M. Wolfrum, "Impact of Gain Dispersion on the Spatio-Temporal Dynamics of Multisection Lasers", *IEEE J. Quantum Electron.*, vol. 37, pp. 183-188, 2001.